catalysts

Review

Sulfide-Based Photocatalysts Using Visible Light, with Special Focus on In_2S_3, SnS_2 and $ZnIn_2S_4$

José C. Conesa

Instituto de Catálisis y Petroleoquímica, CSIC, 28049 Madrid, Spain; jcconesa@icp.csic.es

Abstract: Sulfides are frequently used as photocatalysts, since they absorb visible light better than many oxides. They have the disadvantage of being more easily photocorroded. This occurs mostly in oxidizing conditions; therefore, they are commonly used instead in reduction processes, such as CO_2 reduction to fuels or H_2 production. Here a summary will be presented of a number of sulfides used in several photocatalytic processes; where appropriate, some recent reviews will be presented of their behaviour. Results obtained in recent years by our group using some octahedral sulfides will be shown, showing how to determine their wavelength-dependent photocatalytic activities, checking their mechanisms in some cases, and verifying how they can be modified to extend their wavelength range of activity. It will be shown here as well how using photocatalytic or photoelectrochemical setups, by combining some enzymes with these sulfides, allows achieving the photo-splitting of water into H_2 and O_2, thus constituting a scheme of artificial photosynthesis.

Keywords: photocatalysis; sulfides; visible light; dye removal; environment protection; disinfection; water splitting; CO_2 reduction

Citation: Conesa, J.C. Sulfide-Based Photocatalysts Using Visible Light, with Special Focus on In_2S_3, SnS_2 and $ZnIn_2S_4$. *Catalysts* **2022**, *12*, 40. https://doi.org/10.3390/catal12010040

Academic Editors: Ewa Kowalska, Wonyong Choi, Detlef W. Bahnemann, Ioannis Konstantinou, Vincenzo Vaiano, Magdalena Janus and Zhi Jiang

Received: 4 July 2021
Accepted: 27 December 2021
Published: 30 December 2021

1. Introduction

Photocatalysts are used for many purposes: energy-related applications, fine chemicals synthesis, environment protection, or detection of specific chemicals. Photocatalysis has been known for a long time. The first work on heterogeneous photocatalysis (to this author's knowledge) was reported by Moore and Webster in 1913 [1]. The photoreduction to formaldehyde of CO_2 was described there, using iron or uranium oxide colloids and utilizing visible light. Since there is currently an urgent need to revert the increase of CO_2 in the atmosphere, this was certainly an important work. This paper appeared just after the work by G. Ciamician [2], which said in its last sentences, "So far, human civilization has made use almost exclusively of fossil solar energy. Would it not be advantageous to make better use of radiant energy?" Almost six decades later, an article was published by Fujishima and Honda [3] who proposed using photoelectrochemistry, a practical way to photodissociate H_2O into O_2 and H_2.

Those authors used a single crystal of rutile TiO_2 in their work. Given that its bandgap is 3.0 eV, it absorbs light in the near-UV range, thus it is unsuitable for converting much of the solar spectrum. Other oxides like $SrTiO_3$, ZnO, or anatase TiO_2, having bandgaps above 3.0 eV, have a similar limitation; nonetheless, for some fine chemical syntheses and especially for environment protection, anatase-type TiO_2 remains unsurpassed as photocatalyst. Other materials have been tried in order to enlarge the amount of solar spectrum that can be used. Thus, anatase has been doped with cations or anions, and completely different oxides have been developed like $BiVO_4$ (with E_g = 2.4 eV); this material, which is mentioned frequently as able to photogenerate O_2, as well as the oxides mentioned before with bandgaps higher than 3.0 eV, are certainly resistant to photocorrosion. Additionally, (oxy)sulfides [4–7], (oxy)nitrides [8–11], selenides [12–15], several varieties of doped carbons [16–19], and a few more exotic materials were proposed in order to use a larger range of the solar spectrum. On the other hand, for energy applications, a co-catalyst is frequently required to facilitate the O_2 and/or H_2 evolution, the CO_2 reduction or the conversion of substances derived from biomass.

Many such materials can be also used in photoelectrochemical (PEC) systems. For example, Fe_2O_3 in the hematite phase (see structure in [20]) has a small mobility of the photogenerated current carriers so that high recombination rates occur unless a very small thickness is used; it is, however, very actively studied for PEC uses thanks to its convenient bandgap (≈1.9 eV) and especially its abundance. Additionally, this material is resistant to photocorrosion. Examples of its use in photocatalysis can be found [21–23].

This review deals with the use of sulfide photocatalysts, which in many cases can use visible light (even infrared light in some cases). Many reviews have appeared dealing with photocatalysis using sulfides for protection of the environment [24] and transformation of organic molecules [25], as well as others dealing with more general photocatalysts (including sulfides), devoted to H_2 generation [26,27] and CO_2 reduction [28]; sulfides containing several cations have been also studied for photocatalysis or energy harvesting purposes [29,30]. Mixing sulfides with other phases has been utilized as well to better separate the photogenerated holes and electrons (leading, when both semiconductors absorb light, to the so-called Z-scheme) [31].

It is well known that sulfides, particularly in oxidizing conditions, can be photocorroded; efforts are thus made in order to avoid or at least minimize this process [32]. Therefore, sulfide photocatalysts are mainly used for photoreduction processes, as is the case of H_2 generation or CO_2 reduction. This might require using a sacrificial agent, e.g., sulphite or sulfide anions, which makes the process useful only for basic studies, except if the sacrificial agent is derived from biomass.

1.1. 2-Fold Coordinated Sulfides

One 2-fold coordinated sulfide that has been studied for photocatalysis is HgS (cinnabar). Its structure is given in [33]; its bandgap is 2.05 eV, as shown in [34]. Some other results in photocatalysis by HgS, combined with other phases, are found in [35,36].

1.2. Tri- and Tetrahedrally Coordinated Sulfides

There are some sulfides which contain cations in trigonal planar coordination. For example, Bi_2S_3, with both 4- and 3-fold coordinated Bi (due to a lone pair present in Bi; its structure is reported in [37]). Its bandgap is 1.3–1.7 eV and has been used for photocatalysis either alone [38,39] or in combination with other phases [40–42]. An additional example is CuS with covellite structure (structure reported in [43]), which also has Cu in trigonal and tetrahedral coordination. Its bandgap is 1.75 eV and has also been used alone [44,45] or combined with other materials, for photocatalysis applications [46–48]. It must be noted that, in spite of its formula, it contains mainly Cu^+ [49], which means that disulfide ions exist in it.

Additionally, Ag_2S (structure reported in [50]) and Cu_2S (structure reported in [51]) contain, in their most stable phases, trigonally coordinated cations and have been used as well as photocatalysts. For example, Cu_2S, which has a bandgap (indirect) of 1.2 eV [52], was utilized in degradation of herbicides combined with Bi_2WO_6 [53], in degradation of dyes in combination with TiO_2 of P25 type [54] or with H_2O_2 [55]; combined with MoO_3, it has been used for H_2 generation, degradation of dyes, or reduction of Cr (VI) [56]. Ag_2S, in turn, has an indirect bandgap of 1.0 eV [57]; it has been utilized as a photocatalyst in a number of composites for generation of H_2 [58], degradation of dyes, or reduction of CO_2 [59], as well as in disinfection [60]. Several $Cu_{2-x}S$ structures were used as well as photocatalysts [61].

A significant amount of sulfides contain only tetrahedrally coordinated cations. This is the case, for example, of ZnS (structure reported in [62]). It has a rather large bandgap (3.4 eV [63]), so that it can absorb only light in the UV range. It has been used, however, in photocatalysis for very different applications [64–66]. Note that this material can adopt different shapes, influencing its photocatalytic and photophysical properties [67].

The sulfide most studied for photocatalysis is probably CdS (structure reported in [68]), also tetrahedrally coordinated. Due to the high mobility of its photo-excited electrons and holes, and its significant ability to absorb light in the visible range ($\lambda < 500$ nm; its bandgap is 2.48 eV [63]), several reviews have studied its capabilities for generation of H_2 [69], organic chemistry transformations [25] or degradation of dyes [24]. One problem is the toxicity of Cd; this sulfide is also prone to photocorrosion, particularly in oxidizing conditions [70]. Some attempts have been made to decrease this effect [71,72]. On the other hand, CdS easily undergoes (as in the case of CdSe) quantum confinement effects. Therefore, its particle size can be tailored by irradiating it with monochromatic light in oxidizing conditions; any photocorrosion will finish when the size of its particles is so small that the single-wavelength light can no longer be absorbed [73].

Another class of tetrahedrally coordinated sulfide photocatalysts that are studied include the chalcopyrite family. Thus, $AgGaS_2$, $CuGaS_2$, and $CuInS_2$, all of them with chalcopyrite structure (see structure for $AgGaS_2$ in [74]), have gaps of 2.6, 2.3, and 1.5 eV, respectively, and even their alloys have been used as photocatalysts. $CuGaS_2$ [75,76], (Ag,Cu)GaS_2 [77] or (Ag,Cu)(In,Ga)S_2 [78] as well as doped $AgGaS_2$ [79] are active for photogeneration of H_2; mixing $CuGaS_2$ with RGO-TiO_2 has photocatalytic activity in reducing CO_2 to CO [80]. Some systems of this kind can be used for the photocatalytic elimination of dyes [81], nitrate ions [82] or NO [83]; several years ago, a review dealt with the photocatalytic uses of $CuInS_2$ [84]. Additionally, kesterites, which have structures similar to chalcopyrites (see [85]) and have a bandgap of 1.5 eV (like $CuInS_2$), were used as well as photocatalysts [86].

1.3. Sulfides including 6-Fold Coordinated Cations

Materials that have been studied extensively as photocatalysts are WS_2 and (especially) MoS_2; there are several recent reviews on them [87–89]. They have layered structures with cations in prismatic coordination, held together by van der Waals forces (see their 2H structures in [90,91], respectively). They are also polymorphs [92,93]) and have indirect bandgaps of 1.35 eV and 1.23 eV, respectively [94]. These bandgaps can be increased by decreasing their particle sizes; in fact, isolated trilayers of MoS_2 and WS_2 have, according to photoluminescence data, direct bandgaps of respectively 1.89 and 2.03 eV [95]. This might position their conduction bands to levels more negative than the $H_2|H^+$ electrode potential [96], so that H_2 photogeneration might be facilitated. MoS_2 with small-to-moderate particle size. is much more efficient photocatalytically if its particle size falls below 4–5 nm [97,98]; this is certainly a quantum confinement effect. It must be noted, on the other hand, that there is another structure of MoS_2, termed 1T, which has octahedral, not prismatic, coordination (see structure in [99]). It has metallic characteristics, so that it is very active in combining protons to achieve H_2 evolution [100].

Other 6-fold coordinated sulfides have been studied for photocatalysis. This is the case of ZrS_2 (see structure in [101]), which is also a layered structure held together by dispersion forces, but it has octahedral, not prismatic, coordination, at difference with 2H MoS_2 or WS_2 (i.e., it is similar to 1T MoS_2). Its bandgap is ca. 1.7 eV [102]; however, as shown in [103] if it is made in 2–3-layer shape, it may attain a 2.0 eV bandgap making it ideal for photo-generation of H_2 [103]. HfS_2 has a similar structure [101] but has a smaller bandgap [104]. Its isolation from ZrS_2 is difficult, however, and it has therefore rarely been used in photocatalysis [105].

Additionally, FeS_2 with pyrite structure (including, in this case, only disulfide ions [106]) also has an octahedral coordination to S atoms; its bandgap is 0.95 eV and has been used sometimes for photocatalysis [107].

Finally, there is another octahedrally coordinated sulfide: PbS (its structure can be found in [108]). However, its bandgap is rather small (ca. 0.5 eV or less, as shown in [109]). Still, it has been considered for photocatalysis in combination with other phases [110,111].

This work will concentrate in the experience of our lab with three simple sulfides including octahedral coordination: In_2S_3, SnS_2, and $ZnIn_2S_4$. They will be considered alone or with additions making them more photocatalytically active. It must be noted, therefore, that this review puts a special emphasis on the author's own work.

2. Discussion and Comments on Previous Results of Our Group

2.1. In_2S_3

This material has a cation-defect spinel lattice (see its β structure in [112]; when the tetrahedral cations are disordered, the structure is named α) and a direct bandgap of 2.0–2.1 eV. It is frequently used as buffer layer in thin film photovoltaic cells. It has been used for H_2 photoproduction in works beginning 15 years ago [113–115]. Its use for aqueous organics photodegradation is also relatively old [116–118]. Some 315 articles on the photocatalytic use of In_2S_3 (or its combination with other phases) have appeared until now, being combined frequently with TiO_2 as well for dye or antibiotics degradation [119,120], H_2 photogeneration, [121] or elimination of warfare agents [122]. Some recent reviews on the photocatalytic utilization of In_2S_3 have appeared [123,124].

2.1.1. Photocorrosion Resistance and Spectral Response of In_2S_3

We examined these aspects in a former work [125]. In_2S_3 was hydrothermally synthesized, and its specific surface ($S_{BET} \approx 40\ m^2/g$) was characterized; XRD revealed β-In_2S_3 with disordered cation vacancies, and diffuse reflectance spectroscopy confirmed the 2.1 eV bandgap. This sulfide was tested in the photocatalytic degradation of aqueous HCOOH, showing that In_2S_3 is more active (Figure 1a) and photocorrosion-resistant (Figure 1b) than CdS. Its spectral response was shown, using a series of λ-selecting filters, to agree with the bandgap (Figure 1c). The HCOOH degradation mechanism coincided with Equation (1) of [125].

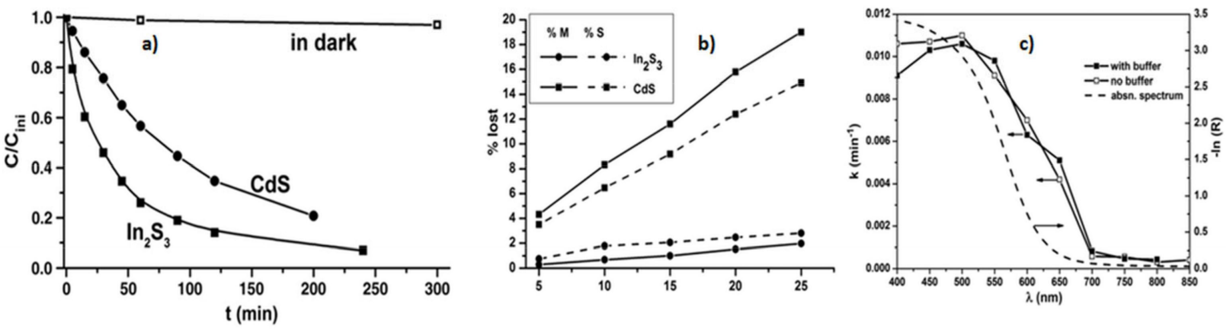

Figure 1. Photocatalytic use of In_2S_3 for degrading aqueous HCOOH: (**a**) activity compared with CdS; (**b**) resistance to photocorrosion (from chemical analysis of S and metal ions gone into solution) compared with that of CdS; (**c**) spectral response of In_2S_3 in this process, evaluated through its first order rate constant, compared with the diffuse reflectance spectrum of the material (Adapted from Ref. [125]).

2.1.2. Mechanism Research in the Degradation of the Dye Rhodamine B

The use of In_2S_3 for degrading this dye photocatalytically started more than 10 years ago [126]. This subject was undertaken by us recently [127], using the same hydrothermal method for making In_2S_3 and trying to better assess the mechanism of this process. The same nanocrystalline In_2S_3 was used as in the preceding section, using it now in degrading the rhodamine B dye. The evolution of the light absorption at λ = 554 nm of this dye in water solution (once the photocatalyst was filtered out), given in Figure 24.10 of [127], verified that higher wavelengths implied smaller activity in photocatalytic action.

The experiment revealed as well that the dye degradation involved more than two intermediate products, since no isosbestic point appeared in the absorption spectra of the solution. Besides, the evolution of the photodegradation depended on the presence of O_2, as shown in Figure 2; with O_2 the decay is much faster, while under N_2 the component absorbing light at lowest wavelength takes much longer to be eliminated.

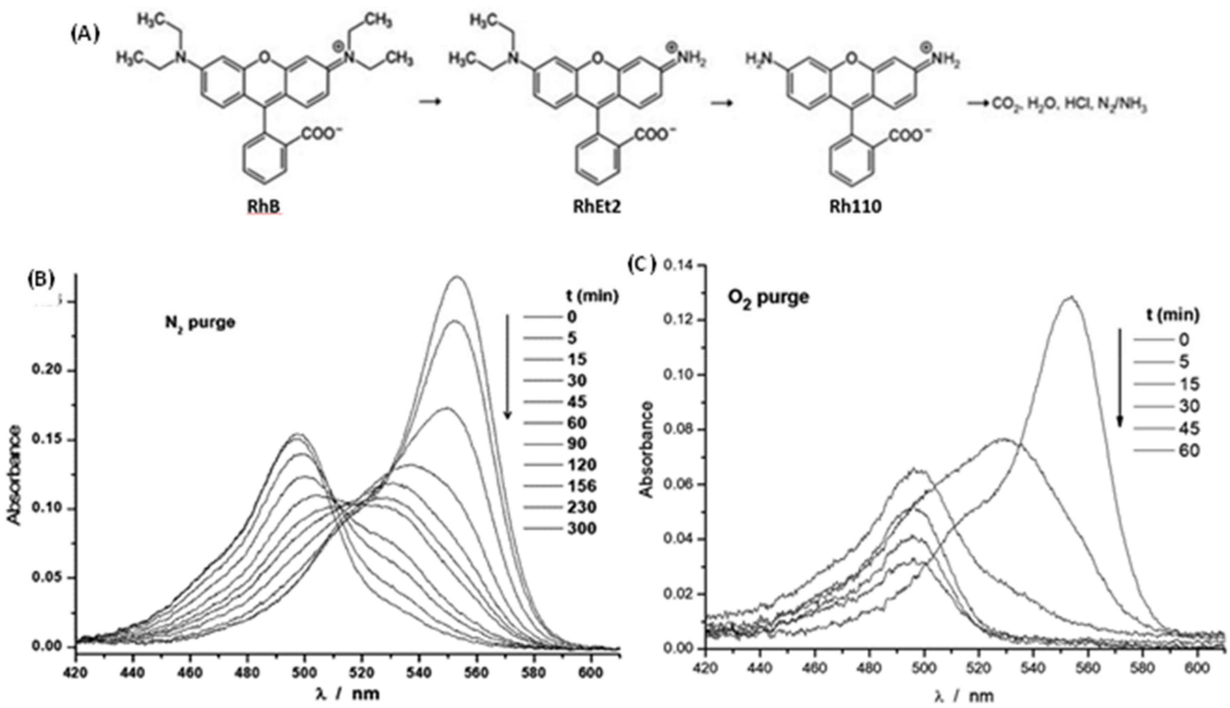

Figure 2. (**A**) Mechanism of the RhB degradation. Evolution of the absorption of light by the RhB dye (or by its intermediate degradation products) at different times under N_2 (**B**) or O_2 (**C**) flow (Adapted from Ref. [127]).

To understand this behavior, a principal component analysis (PCA) [128] of the absorption spectra of the dye was carried out. This allowed determining, first, that only three independent factors explained all the dye spectra. Besides the initial RhB dye, only another two components (by comparison with literature data) could be assigned: the same dye fully de-ethylated in just one N atom, or in both N atoms (leading to dye Rh110). The degradation steps sequence could be thus established:

Furthermore, with no O_2 present, the last RhB degradation step in which the aromatic ring is broken takes much longer (see Figure 2). This implies that this step depends on the presence of $O_2H^\bullet$ or O_2^- radicals, formed by transfer to O_2 of photogenerated electrons and subsequent protonation. The precedent steps involve thus the more aggressive $OH^\bullet$ radicals (due to transfer of holes from In_2S_3). These $OH^\bullet$ radicals might well survive much shorter time in solution; if the adsorption of the dye on In_2S_3 occurs mainly through the ethyl residues, once these disappeared the molecule fully de-ethylated, it may go mostly into solution, and there it may react only with the $O_2H^\bullet$ or O_2^- radicals, known to have longer lifetimes. The final part of that study involved decomposing with PCA also the dye absorption spectra found using the wavelength-selecting filters while bubbling the irradiated solution with O_2; the results are shown in Figure 3.

Undertaking a semilogarithmic plot fitting of the initial RhB dye decays obtained in Figure 3 allowed determining the spectral response of that decay. It is shown in Figure 4, evidencing the agreement of this profile with the In_2S_3 absorption spectrum (not of the dye).

2.1.3. Two-Photon Processes Using V-Substituted In_2S_3

A proposal was made some years ago stating that by insertion of a narrow, delocalized band (partially filled) between the valence (VB) and conduction (CB) bands of a semiconductor could allow realizing electron transfers, using sub-bandgap photons from the VB to the CB in two steps, thus enhancing the theoretical photovoltaic efficiency beyond the Shockley–Queisser limit [129]. Several researchers (including this author) studied with DFT calculations how to achieve such structure (see [130] and references therein). This last work showed that by substituting with vanadium part of the In atoms in In_2S_3 could provide a proper structure to achieve this purpose.

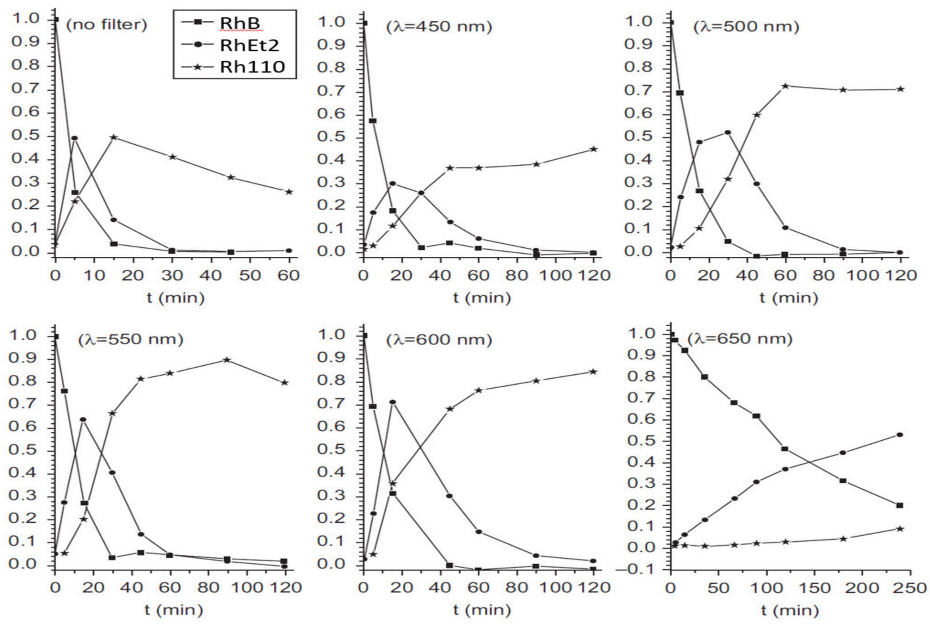

Figure 3. PCA analysis results: evolution of the RhB dye and products RhEt2 and Rh110 irradiated in presence of In_2S_3 with light unfiltered or using band-pass filters of wavelength λ. Results scaled relative to the dye absorption at t = 0 (Adapted from ref. [127]).

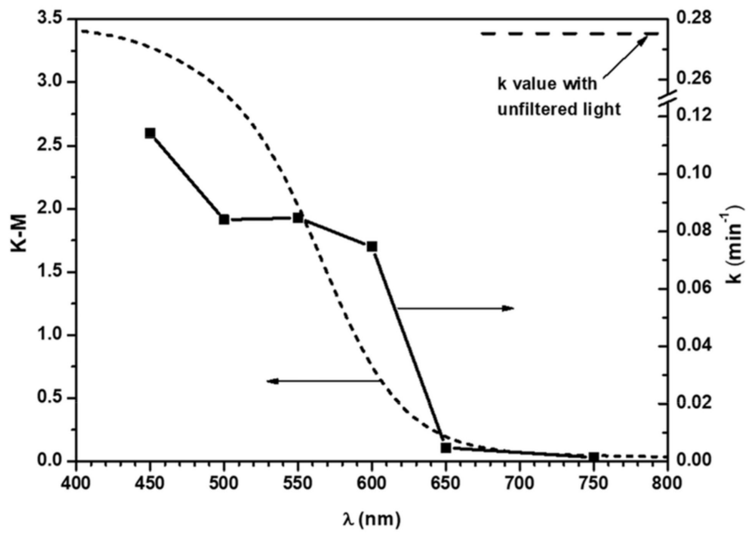

Figure 4. Spectral response of the initial RhB dye degradation (Adapted from Ref. [127]).

Then, our laboratory carried out the preparation of this material, achieving it shortly after [131]. Here the VCl_3 compound used reacted with protons generating much H_2; a water- ethylene glycol (with 10% water) was therefore used, to decrease that reaction. The V^{4+} ions in the material, detected with EPR, were thanks to this strategy below 25%. We then tested it later in photocatalysis using the same aqueous HCOOH degradation reaction [132]. The results indicated (Figure 5a) that the HCOOH degradation spectral response was extended to longer wavelengths.

The most interesting result was provided by photoluminescence (PL) tests. These verified that while PL at ~600 nm (which corresponds roughly to the In_2S_3 gap) were excited in V-free In_2S_3 only by shorter wavelengths (as expected), the PL at that same wavelength could be excited in V-containing In_2S_3 also with wavelengths longer than the In_2S_3 bandgap. V-free In_2S_3 was unable to act in the same manner. (Figure 5b), evidencing an upconversion process requiring two photons. Furthermore, the range in which the PL was excited was the same as that in which photocatalysis took place (compare Figure 5a,c), proving that the process provoking this upconversion made possible as well the migration of holes and electrons to the surface, leading to chemical reactions. This was not due to a nonlinear process, as shown in Figure 5d, evidencing that PL does not depend on the degree of filling of the first transition, in agreement with both Figure 5e and the scCOHSEX + G_0W_0 result shown in Figure 7a of [132].

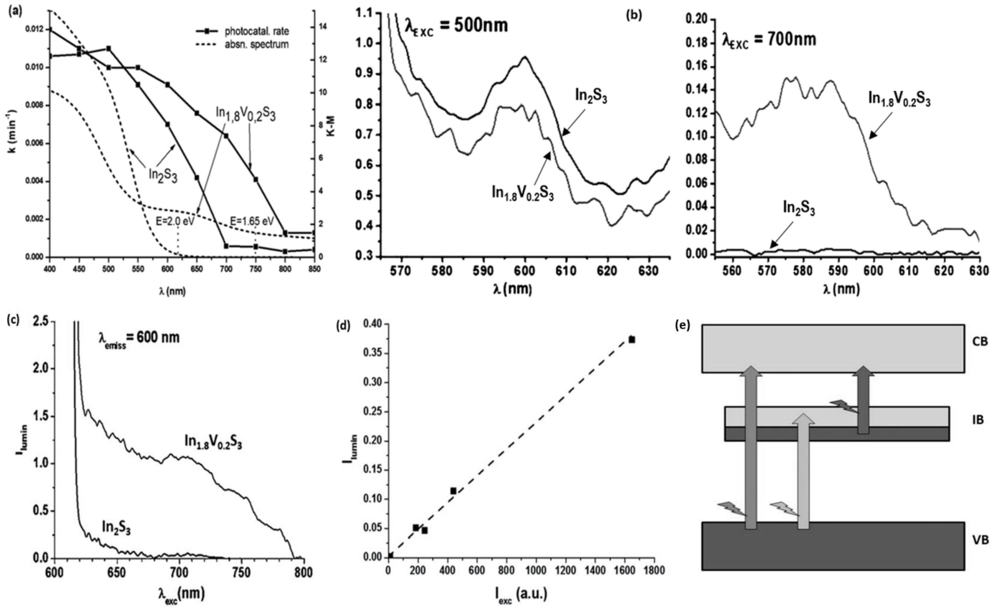

Figure 5. (**a**) Spectral response of aqueous formic acid degradation of V-containing In_2S_3, compared with that of V-free In_2S_3 and with their respective absorption spectra. (**b**) PL tests using wavelengths above and below the bandgap energy; only V-containing In_2S_3 can excite PL at near 600 nm, while In_2S_3 cannot. (**c**) PL range in which emission at λ = 600 nm is excited only by V-containing In_2S_3. (**d**) Linear relationship between excitation intensity and resulting photoluminescence, which is in agreement with (**e**) (Adapted from Ref. [132]).

PL tests with terephtalic acid, which reacts with OH radicals to form the corresponding PL-active derivative (which has photoluminescence properties), showed as well (Figure 6) that the generation of these radicals (as shown in earlier work using also In_2S_3 [117]) occurs as well for longer wavelengths in the case of V-containing In_2S_3.

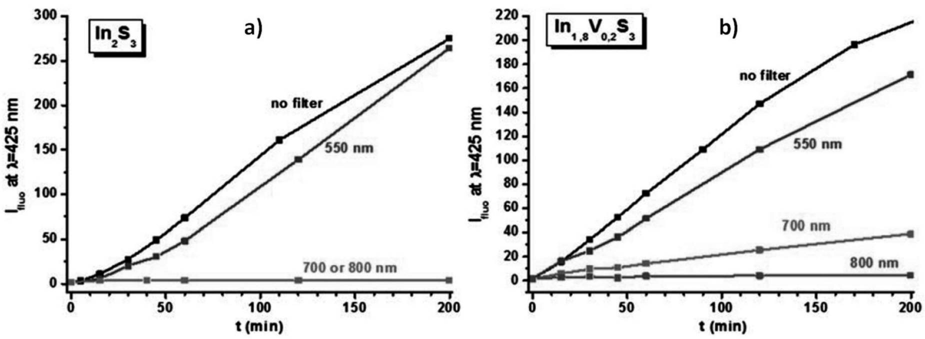

Figure 6. Increase in the fluorescence of hydroxy−terephtalic acid, detected at 425 nm, observed by irradiation at λ = 700 nm not in the case of (**a**), i.e., In_2S_3, while V−containing In_2S_3 (**b**) does show it (Adapted from Ref. [132]).

2.1.4. Photocatalytic Generation of H_2 with an In_2S_3-Hydrogenase Combination

Hydrogenases are electroactive enzymes which contain dinuclear Ni-Fe or Fe-Fe complexes, bonded mainly to sulfur atoms, catalyzing efficiently the reaction

$$2\,H^+ + 2\,e^- \leftrightarrow H_2 \quad (1)$$

We thus published a work recently [133] in which a Ni-Fe hydrogenase, inserted in a hydrothermally prepared porous In_2S_3 structure (having a S_{BET} area similar to that in [125]), was suspended in a sodium sulfite aqueous solution (used as sacrificial reagent) and irradiated then with white light. H_2 was produced and detected with MS, as shown in Figure 7a), only when the In_2S_3 suspension at 37 °C and pH = 7 was irradiated in presence of the hydrogenase, behaving thus as co-catalyst. Comparing this production of H_2 with that resulting when the hydrogenase, when no irradiation nor In_2S_3 were present, was contacted with a solution of reduced methylviologen (a very good substrate for generation of H_2 with this enzyme), indicated a similar ability for generation of H_2 in both cases (Figure 7b). This means that electrons photogenerated in In_2S_3 can be efficiently transferred to the enzyme, the latter being thus able to produce H_2.

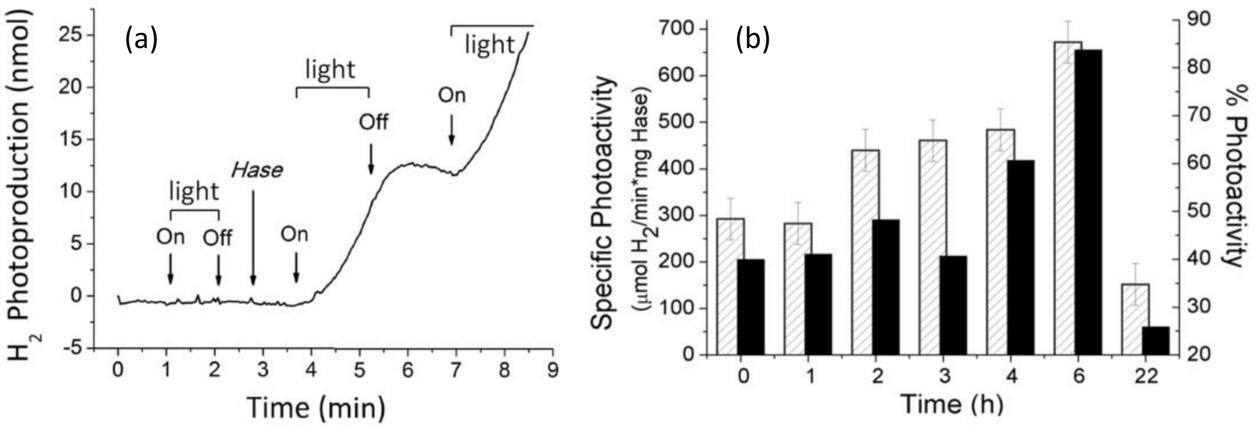

Figure 7. (**a**) H_2 production by light when both In_2S_3 and hydrogenase are present. (**b**) H_2 production by irradiated In_2S_3-hydrogenase for several incubation times (striped columns) and % of H_2 production by this same system, compared with the H_2 formed after equal incubation times, in presence of MV^+ and hydrogenase when no light nor In_2S_3 are present (black columns) (Adapted from Ref. [133]).

2.1.5. Photoelectrochemical Generation of O_2 by an Electrode including Laccase and In_2S_3

Laccases are enzymes, which contain Cu-oxide clusters, the normal role of which is reducing O_2 to water without stopping at the H_2O_2 intermediate product. Previous experience of another group in our institute [134] showed that the reverse reaction, i.e., direct evolution of O_2 from water, could be carried out as well. We thus linked a laccase to an electrode and could verify how the same could be carried out irradiating an electrode which contained a visible light-responsive semiconductor (In_2S_3) so that an overpotential could be achieved which was lower than that needed for a nonirradiated electrode.

Thus, a recent publication by our group was made [135] using an electrode built by depositing hydrothermally prepared In_2S_3 (again with S_{BET} area similar to that in [125]) on a FTO-covered glass, then linking covalently a laccase enzyme to the semiconductor. Several electrochemical measurements were carried out in phosphate-buffered solution (i.e., pH = 7.1) under Ar atmosphere using an Ag/AgCl reference electrode; a sensor of dissolved O_2 allowed detecting this latter molecule.

Figure 8 gives a summary of the results. Part A shows cyclic voltammograms (CVs) of FTO/In_2S_3/laccase electrodes in the dark (a) and under illumination (b); inset shows the O_2 sensor signal the same conditions (with delay because of the time that O_2 needs to diffuse to the sensor); in the absence of In_2S_3 and/or laccase, the CV current and the signal from the O_2 sensor were rather smaller or even negligeable. No relevant amount of H_2O_2 was found in the solution, evidencing the known ability of this laccase to catalyze the 4-electron process between O_2 and H_2O. Part B shows chronoamperograms recorded at 1 V vs. SHE upon irradiation of FTO/In_2S_3 (left) and FTO/In_2S_3/laccase electrodes (right); the O_2 sensor signal is included in both cases. As it can be seen, a significant response of the O_2 sensor appears only in the presence of the laccase enzyme. It could be also verified, after calibration of the O_2 sensor signal, that the total current difference observed in both cases corresponded well with the quantity of O_2 generated if a 4-electron process was assumed (it must be noted that the result observed without laccase corresponds to an electrode capacitance charging effect). On the other hand, in the absence of illumination FTO or FTO/laccase, electrodes require potentials higher that 1.5 V in order to generate some O_2. The system implies, therefore, an overpotential decrease of at least 0.55 V because of the effect of the irradiated In_2S_3 semiconductor.

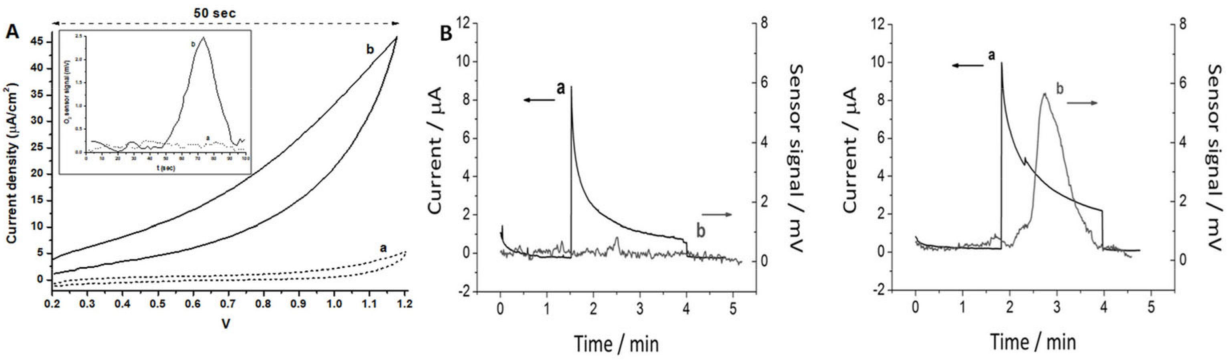

Figure 8. (**A**) Cyclic voltammograms of electrodes in dark (a) and under irradiation (b); the O_2 sensor signal is shown in the inset in both cases. (**B**) Chronoamperograms of electrodes without (left) and with laccase (right) irradiated during ca. 2.3 min, the O_2 sensor signal being also shown (Adapted from Ref. [135]).

We can state that this was the first time ever in which combining an enzyme (used as co-catalyst) and a visible light-sensitive inorganic semiconductor showed ability to generate O_2 upon illumination, as it occurs in natural photosynthesis.

2.2. A Semiconductor Related to In_2S_3: $ZnIn_2S_4$

This material (structure given in [136]; note that the c axis must be that of length 24.68 Å, as this is the one that gives a XRD diffraction compatible with that Figure 24.5 in [127]) has a layered structure, with a central layer of octahedrally coordinated In atoms having at one side a layer of In atoms tetrahedrally coordinated and at the other side a layer of Zn atoms tetrahedrally coordinated; the external atoms are always sulphur. The layers are held together by van der Waals forces; different stackings of them are possible [136–138]. For this material, bandgaps are in the 1.9–2.2 eV range, perhaps because of the several stacking possibilities. There are doubts as to whether this bandgap is direct or indirect, which may be again due to the different layer stackings possible [139,140]. The first work on photocatalysis using this material appeared less than 20 years ago [141]; since then, over 600 studies on its photocatalytic properties have appeared, either for dye degradation [142] or photogeneration of H_2 [143]. Recent reviews of its photocatalytic properties have appeared [140,144].

We decided to undertake a study on its spectral response for photocatalysis; the results were reported in [127]. Its diffuse reflectance spectrum was measured; however, as previously stated, there are some doubts concerning its direct or indirect character. Thus, a DFT calculation using a hybrid functional was carried out, and the result (Figure 9A) shows that it has an indirect gap, but so close to the direct one that except for PL tests the bandgap can be considered direct in Tauc plots; thus a 2.6 eV bandgap was determined.

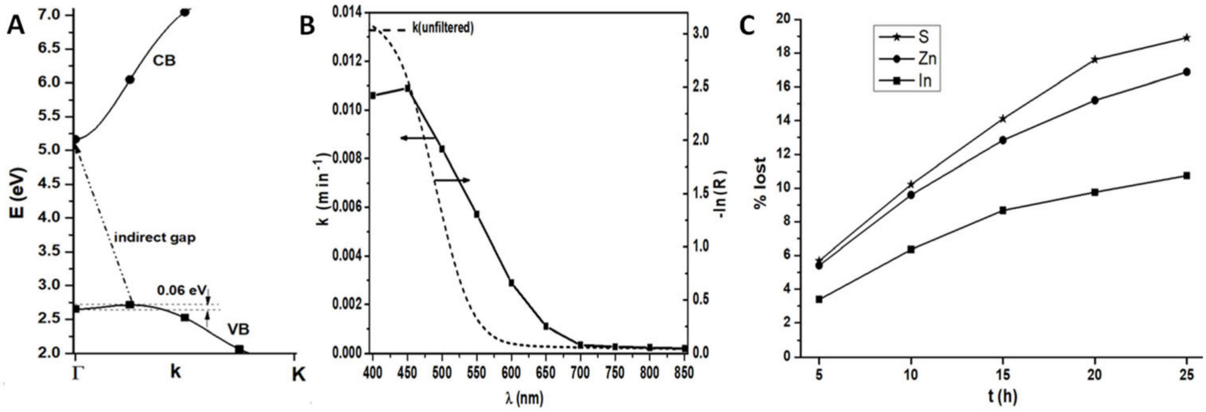

Figure 9. (**A**) Results of a hybrid DFT calculation showing the indirect character of the $ZnIn_2S_4$ bandgap. (**B**) spectral response of $ZnIn_2S_4$ in photocatalytic degradation of aqueous HCOOH, compared with its diffuse reflectance absorption spectrum. (**C**) Time dependence of $ZnIn_2S_4$ photocorrosion during HCOOH photocatalysis: amount of each element gone into solution, as verified with chemical analysis (Adapted from Ref. [127]).

The photocatalytic spectral response of $ZnIn_2S_4$ was determined, like for In_2S_3, by means of the degradation rate of an HCOOH aqueous solution using a stirred suspension of $ZnIn_2S_4$, after verifying its crystallinity and S_{BET} surface area (37.4 m^2/g). The results, given in Figure 9B, show again that a good ability to absorb visible light makes this material interesting. However, its rate of photocorrosion is rather larger than that of In_2S_3 (Figure 9C), perhaps due to the presence of tetracoordinated Zn in one side of the layers (actually, the Zn fraction gone into solution is higher than that of In).

2.3. *SnS_2*

This material (structure in [145]), which contains only octahedrally coordinated Sn, has as well a layered structure, in which each S-Sn-S trilayer is bonded to the next one by weak van der Waals forces, leading thus again to several stacking possibilities [146,147]. Its most stable phase has an indirect bandgap of 2.2 eV [148]; it can thus absorb a significant amount of visible light.

SnS_2 has thus been studied for photocatalysis. The first publication of its photocatalytic properties appeared less than 15 years ago [149]; ca. 600 publications on these properties have appeared since then, related to H_2 generation or dye degradation [150], but also publications on less common processes such as Cr(VI) photoreduction [151], removal of antibiotics [152], or reduction of CO_2 to CH_4 [153] or CO [154] have appeared. Works on photocatalysis using SnS_2 done by our group are presented here.

2.3.1. SnS_2 Spectral Response

In our group, we tested its spectral response [155] using once more the photodegradation of HCOOH dissolved in water using a stirred suspension. The material, synthesized with a hydrothermal method, achieved a rather good crystallinity, with a S_{BET} area of 36 m^2/g. Tauc plots derived from its diffuse reflectance spectrum provided a bandgap of 2.25 eV, thus agreeing well with literature.

It was verified that this semiconductor is clearly more active than CdS, as shown in Figure 10A. Using monochromatic light allowed verifying its spectral response as well; this is shown in Figure 10B together with the absorption spectrum of SnS_2. One can see again that this material is active in photocatalysis in all the wavelength range in which it absorbs light. Even more interesting is its high resistance to photocorrosion, being much higher than that of CdS as evidenced in Figure 10C; this may be related to the higher cation charge and the octahedral coordination of SnS_2, which may lead to a higher Madelung constant and consequently to a higher cohesion energy.

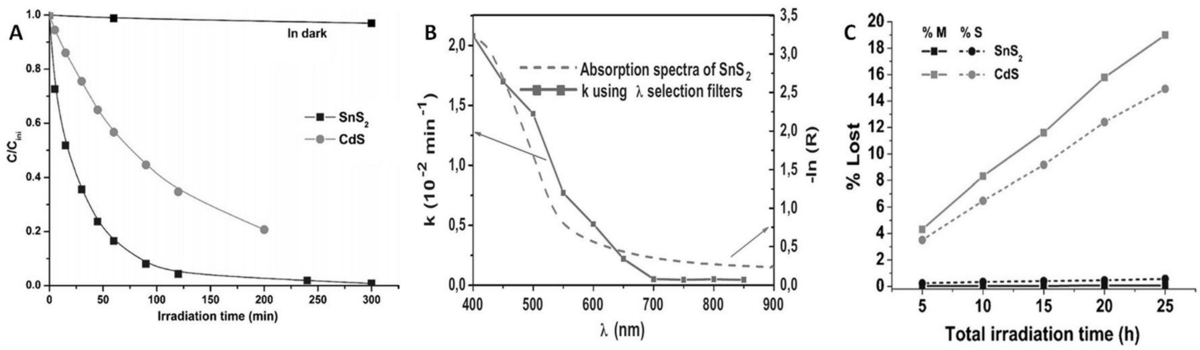

Figure 10. (**A**) Comparison of the aqueous HCOOH photodegradation activity between SnS_2 and CdS; (**B**) SnS_2 spectral response in the same process; (**C**) comparing the photocorrosion rate, evaluated from the amount of the sulfide components appearing in the solution, between CdS and SnS_2 (Adapted from Ref. [155]).

2.3.2. Two-Photon Processes Using V-Substituted SnS_2

As in the case of V-substituted In_2S_3, DFT calculations indicated that V-substituted SnS_2 could lead to two-photon processes. Therefore, the synthesis of such material was undertaken with success [156]. A summary of the obtained results is presented below.

EPR spectroscopy verified that over 90% of vanadium was in the V^{4+} state, as was assumed in the DFT calculations. The spectral response for the photocatalytic degradation of HCOOH dissolved in water using a suspension of V-free and V-substituted SnS_2 is presented in Figure 11, showing again that this response is extended to longer wavelengths, as expected if V introduces an intermediate band in the gap. In this case, however, photoluminescence tests cannot prove an upconversion processes, because SnS_2 is an indirect bandgap semiconductor; the recombination of photoproduced holes and electrons requires phonon participation, therefore the photoluminescence intensity at ambient temperature will be much smaller than for the In_2S_3 case.

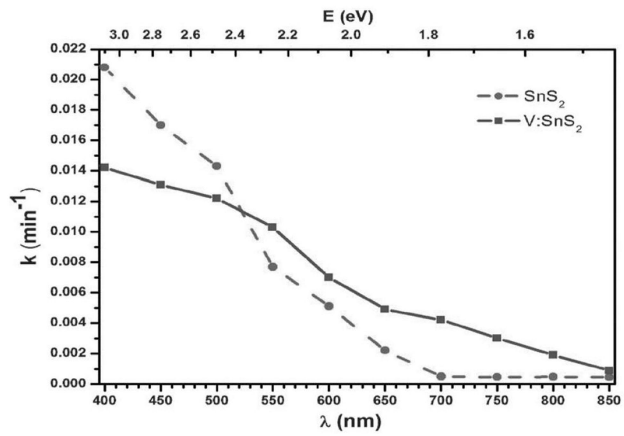

Figure 11. Shift to longer wavelengths of the SnS_2 photocatalytic response when part of the Sn cations are substituted by V cations (Reproduced from Ref. [156]).

It could be thus that, while DFT calculations predict that an in-gap band due to the inclusion of V would not overlap the conduction or valence bands [156], an overlap might exist after all, so that finally only a bandgap reduction might occur. On the other hand, the spectral response shows not much smaller photocatalytic activity at wavelengths lower than the intrinsic bandgap of V-free SnS_2; this suggests that the much lower mobility expected for V-centered sites would not play a significant role, implying that a 2-photon process does occur in this V-containing SnS_2.

2.3.3. Photoelectrochemical Generation of O_2 by a SnS_2 Electrode including a Laccase

That study was carried out by our group as well [157]. A FTO electrode was again used, covered this time by hydrothermally prepared SnS_2 (with S_{BET} area similar to that in [155]); as in our similar study involving In_2S_3, the same laccase enzyme was covalently linked to it. In this case the electrical contact was improved by including on top of the SnS_2 nanoparticles ITO nanoparticles (ITOnp) at 1% level. Electrochemical tests were carried out, monitoring the dissolved O_2 amounts with the same sensor. Ethanol, phosphate buffer at pH = 7.0, and acetate buffer at pH = 4.2 were the tested solvents.

The best results were achieved with the acetate buffer. Figure 12(Aa) shows that O_2 appeared only when the electrode was illuminated; trace b shows the same electrode without the laccase enzyme bonded to it. In the absence of laccase, a higher photo current was detected; this might be due to a stronger SnS_2 photocorrosion, due to its inability to transfer to the solution the photogenerated holes when the laccase co-catalyst was absent. With the laccase present one can expect that SnS_2 will be more resistant to photocorrosion than In_2S_3. Besides, detecting O_2 could be achieved in high yields with applied voltages as low as 0.4 V vs. SHE (see Figure 12B), implying a high decrease in the overpotential necessary to generate O_2 under illumination; the faradaic efficiency could then reach levels as high as 75%, implying that with these smaller applied potentials the SnS_2 photocorrosion is much decreased. This can be compared with another work showing the photoelectrochemical oxidation of water using as well SnS_2, but now with a Pt co-catalyst to aid the same reaction [158].

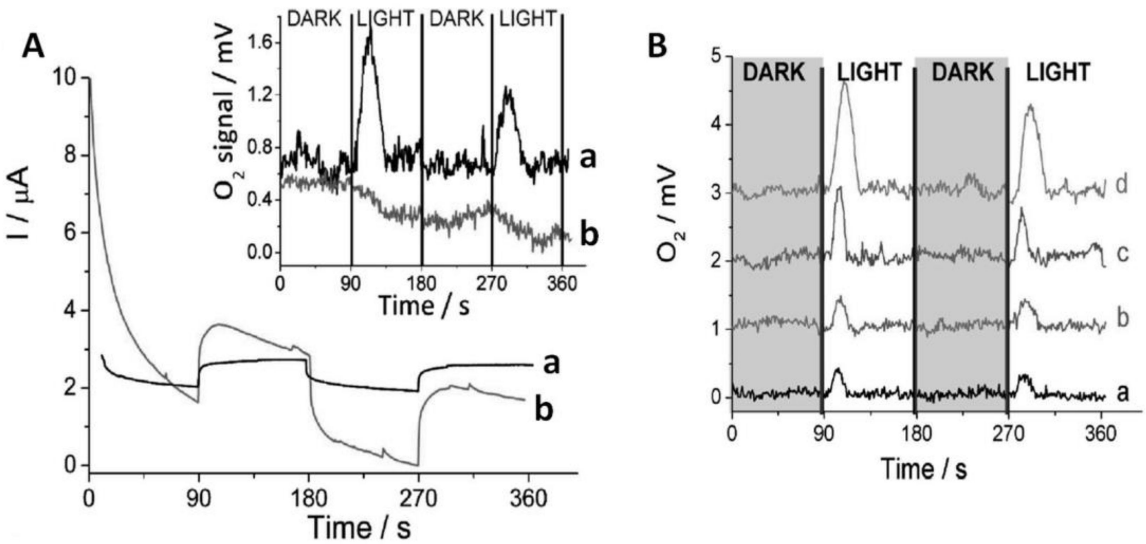

Figure 12. (**A**) Photoelectrochemical data obtained with FTO/SnS_2/ITOnp electrodes, polarized at 1V vs. SHE: (a) with laccase enzyme; (b) without it. The inset presents the simultaneous O_2 generation in this experiment. (**B**) O_2 sensor signal for FTO/SnS_2/laccase/ ITOnp electrodes when polarized at (a) 1 V, (b) 0.8 V, (c) 0.6 V, and (d) 0.4 V vs. SHE. Alternating dark/light periods were used in all cases (Adapted from Ref. [157]).

2.4. In_2S_3 and SnS_2 Band Alignment with O_2 and H_2 Standard Potentials

It now must be said whether the conduction bands of In_2S_3 and SnS_2 lie above the H_2 standard potential, so that H_2 can be generated, and whether their valence bands lie below the O_2 standard potential, so that O_2 may be evolved. Here we have the help of [159], which leads to Figure 13:

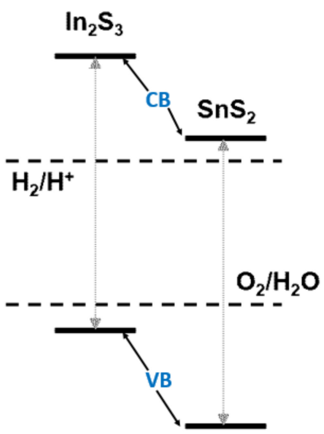

Figure 13. Band alignments respect to the O_2 and H_2 standard potentials.

3. Conclusions

This work has shown that very different sulfides can work as photocatalysts, in some cases combined with other phases, for a number of different reactions like dye degradation, reduction of water or CO_2, herbicide removal, disinfection, or selective organic transformations. One main drawback is the possibility of photocorrosion; this is minimized if the photoreactions involved are reductive ones, or if the holes photogenerated in the system are kept in some oxide phase, e.g., in several Z-scheme combinations [31,46a),53,80]. Thus, the possibility of utilizing sulfide photocatalysts, which can absorb extended ranges of visible light (even near-infrared light in a few cases), is a very interesting alternative.

Funding: This work was made with help of the Programme FotoArt-CM of the Comunidad de Madrid (ref. S2018/NMT-4367).

Acknowledgments: Thanks are given to CSIC for the use of its parallel computer *trueno* in the hybrid DFT calculations.

Conflicts of Interest: The author declares no conflict of interest.

References

1. Moore, B.; Webster, T.A. Synthesis by sunlight in relationship to the origin of life. Synthesis of formaldehyde from carbon dioxide and water by inorganic colloids acting as transformers of light energy. *Proc. R. Soc. Lond.* **1913**, *87*, 163–175.
2. Ciamician, G. The Photochemistry of the Future. *Science* **1912**, *36*, 385–394. [CrossRef]
3. Fujishima, A.; Honda, K. Electrochemical Evidence for the Mechanism of the Primary Stage of Photosynthesis. *Bull. Chem. Soc.* **1971**, *44*, 1148–1150. [CrossRef]
4. Zhao, W.; Maeda, K.; Zhang, F.X.; Hisatomi, T.; Domen, K. Effect of post-treatments on the photocatalytic activity of $Sm_2Ti_2S_2O_5$ for the hydrogen evolution reaction. *Phys. Chem. Chem. Phys.* **2014**, *16*, 12051–12056. [CrossRef]
5. Jiang, L.S.; Li, J.; Li, Y.; Wu, X.Y.; Zhang, G.K. Promoted charge separation from nickel intervening in $[Bi_2O_2](2+)$ layers of Bi_2O_2S crystals for enhanced photocatalytic CO_2 conversion. *Appl. Catal. B* **2021**, *294*, 120249. [CrossRef]
6. Tadesse, S.F.; Kuo, D.H.; Kebede, W.L.; Duresa, L.W. Synthesis and characterization of vanadium-doped Mo(O,S)(2) oxysulfide for efficient photocatalytic degradation of organic dyes. *New J. Chem.* **2020**, *44*, 19868–19879. [CrossRef]
7. Kabbour, H.; Sayede, A.; Saitzek, S.; Lefevre, G.; Cario, L.; Trentesaux, M.; Roussel, P. Structure of the water-splitting photocatalyst oxysulfide alpha-$LaOInS_2$ and ab initio prediction of new polymorphs. *Chem. Commun.* **2020**, *56*, 1645–1648. [CrossRef]
8. Takata, T.; Pan, C.S.; Domen, K. Recent progress in oxynitride photocatalysts for visible-light-driven water splitting. *Sci. Technol. Adv. Mater.* **2015**, *16*, 033506. [CrossRef]
9. Ahmed, M.; Guo, X.X. A review of metal oxynitrides for photocatalysis. *Inorg. Chem. Front.* **2016**, *3*, 578–590. [CrossRef]
10. Jiang, S.J.; Liu, Y.X.; Xu, J. Rare earth oxynitrides: Promising visible-light-driven photocatalysts for water splitting. *Mater. Adv.* **2021**, *2*, 1190–1203. [CrossRef]
11. Sakar, M.; Prakash, R.M.; Shinde, K.; Balakrishna, G.R. Revisiting the materials and mechanism of metal oxynitrides for photocatalysis. *Int. J. Hydrog. Energy* **2020**, *45*, 7691–7705. [CrossRef]
12. Sobhani, A.; Salavati-Niasari, M. Transition metal selenides and diselenides: Hydrothermal fabrication, investigation of morphology, particle size and and their applications in photocatalyst. *Adv. Coll. Interface Sci.* **2021**, *287*, 102321. [CrossRef] [PubMed]

13. Eftelhari, A. Molybdenum diselenide ($MoSe_2$) for energy storage, catalysis, and optoelectronics. *Appl. Mater. Today* **2017**, *8*, 1–17. [CrossRef]
14. Ghobadi, N.; Chobin, S.; Rezaee, S.; Shakoury, R. Tuning the optical and photocatalytic features of copper selenide prepared by chemical solution deposition method. *Surf. Interfaces* **2020**, *21*, 100706. [CrossRef]
15. Yang, X.; Wu, R.; Liu, H.Y.; Fan, H.M.; Zhang, H.Y.; Sun, Y.F. Amorphous molybdenum selenide as highly efficient photocatalyst for the photodegradation of organic dyes under visible light. *Appl. Surf. Sci.* **2018**, *457*, 214–220. [CrossRef]
16. Putri, L.K.; Ong, W.J.; Chang, W.S.; Chai, S.P. Heteroatom doped graphene in photocatalysis: A review. *Appl. Surf. Sci.* **2015**, *358*, 2–14. [CrossRef]
17. Nguyen, T.H.; Yang, D.; Zhu, B.; Lin, H.; Ma, T.Y.; Jia, B. H Doping mechanism directed graphene applications for energy conversion and storage. *J. Mater. Chem. A* **2021**, *9*, 7366–7395. [CrossRef]
18. Chen, X.F.; Xie, Z.L.; Liang, Y.; Wei, J.; Zhu, Y.G.; Huo, Y.N.; Zhang, X.W.; Wang, H.T. Hybridizing TiO_2 with Nitrogen-Doped Carbon: A New Route to A Highly Visible Light-Active Photocatalyst. *ChemistrySelect* **2017**, *2*, 1565–1572. [CrossRef]
19. Liu, T.; Cui, Z.W.; Zhou, J.; Wang, Y.; Zou, Z.G. Synthesis of Pyridinic-Rich N, S Co-doped Carbon Quantum Dots as Effective Enzyme Mimics. *Nanoscale Res. Lett.* **2017**, *12*, 375. [CrossRef]
20. Blake, R.L.; Hessevick, R.E.; Zoltai, T.; Finger, L.W. Refinement of the hematite structure. *Am. Mineral.* **1966**, *51*, 123–129.
21. Xia, Y.B.; Yin, L.W. Core-shell structured alpha-Fe_2O_3@TiO_2 nanocomposites with improved photocatalytic activity in the visible light region. *Phys. Chem. Chem. Phys.* **2013**, *15*, 18627–18634. [CrossRef] [PubMed]
22. Townsend, T.K.; Sabio, E.M.; Browning, N.D.; Osterloh, F.E. Photocatalytic water oxidation with suspended alpha-Fe_2O_3 particles-effects of nanoscaling. *Energy Environ. Sci.* **2011**, *4*, 4270–4275. [CrossRef]
23. Miao, Y.P.; Yang, P. Decoration of alpha-Fe_2O_3 on Graphene for Photocatalytic and Supercapacitive Properties. *J. Nanosci. Nanotechnol.* **2018**, *18*, 333–339. [CrossRef] [PubMed]
24. Ayodhya, D.; Veerabhadram, G. A review on recent advances in photodegradation of dyes using doped and heterojunction based semiconductor metal sulfide nanostructures for environmental protection. *Mater. Today Energy* **2018**, *9*, 83–113. [CrossRef]
25. Hao, H.; Lang, X. Metal Sulfide Photocatalysis: Visible-Light-Induced Organic Transformations. *ChemCatChem* **2019**, *11*, 1378–1393. [CrossRef]
26. Wang, Z.; Li, C.; Domen, K. Recent developments in heterogeneous photocatalysts for solar-driven overall water splitting. *Chem. Soc. Rev.* **2019**, *48*, 2109–2115. [CrossRef]
27. Chandrasekaran, S.; Yao, L.; Deng, L.; Bowen, C.; Zhang, Y.; Chen, S.; Lin, Z.; Peng, F.; Zhang, P. Recent advances in metal sulfides: From controlled fabrication to electrocatalytic, photocatalytic and photoelectrochemical water splitting and beyond. *Chem. Soc. Rev.* **2019**, *48*, 4178–4280. [CrossRef]
28. Vu, N.-N.; Kaliaguine, S.; Do, T.-O. Critical Aspects and Recent Advances in Structural Engineering of Photocatalysts for Sunlight-Driven Photocatalytic Reduction of CO_2 into Fuels. *Adv. Funct. Mater.* **2019**, *29*, 1901825. [CrossRef]
29. Stroyuk, O.; Raevskaya, A.; Gaponik, N. Solar light harvesting with multinary metal chalcogenide nanocrystals. *Chem. Soc. Rev.* **2018**, *47*, 5354–5422. [CrossRef]
30. Kulkarni, P.; Nataraj, S.K.; Balakrishna, R.G.; Nagaraju, D.H.; Reddy, M.V. Nanostructured binary and ternary metal sulfides: Synthesis methods and their application in energy conversion and storage devices. *J. Mater. Chem. A* **2017**, *5*, 22040–22094. [CrossRef]
31. Di, T.; Xu, Q.; Ho, W.K.; Tang, H.; Xiang, Q.; Yu, J. Review on Metal Sulphide-based Z-scheme Photocatalysts. *ChemCatChem* **2019**, *11*, 1394–1411. [CrossRef]
32. Chen, S.; Huang, D.; Xu, P.; Xue, W.; Lei, L.; Cheng, M.; Wang, R.; Liu, X.; Deng, R. Semiconductor-based photocatalysts for photocatalytic and photoelectrochemical water splitting: Will we stop with photocorrosion? *J. Mater. Chem. A* **2020**, *8*, 2286–2322. [CrossRef]
33. Schleid, T.; Lauxmann, P.; Schneck, C. Roentgenographische Einkristalluntersuchungen an alpha-(HgS) (Zinnober). *Z. Kristallogr.* **1999**, *16*, 95.
34. Selvaraj, R.; Qi, K.; Al-Kindy, S.M.Z.; Sillanpaa, M.; Kim, Y.; Tai, C.W. A simple hydrothermal route for the preparation of HgS nanoparticles and their photocatalytic activities. *RSC Adv.* **2014**, *4*, 15371–15376. [CrossRef]
35. Saini, P.K.; Kumar, N.; Chandra, R.; Nath, M.; Minocha, A.K. Facile synthesis of novel SWCNT/HgS nanohybrid: An effective photocatalyst for degradation of methylene blue. *Mater. Lett.* **2019**, *250*, 5–8. [CrossRef]
36. Wang, Z.H.; Zhu, S.Y.; Zhao, S.P.; Hu, H.B. Synthesis of core-shell Fe_3O_4@SiO_2@MS (M = Pb, Zn, and Hg) microspheres and their application as photocatalysts. *J. Alloys Compd.* **2011**, *509*, 6893–6898. [CrossRef]
37. Tilley, R.J.D.; Wright, A.C. X-ray diffraction and electron microscope study of the Bi_2S_3-$PbBi_2S_4$ system. *J. Solid State Chem.* **1986**, *65*, 45–62. [CrossRef]
38. Luo, Y.; Chen, H.; Li, X.; Gong, Z.; Wang, X.; Peng, X.; He, M.; Sheng, Z. Wet chemical synthesis of Bi_2S_3 nanorods for efficient photocatalysis. *Mater. Lett.* **2013**, *105*, 12–15. [CrossRef]
39. Sang, Y.; Dai, G.D.; Wang, L.X.; Gao, X.Y.; Fang, C.H. Hydrothermal Synthesis of Urchin-like Bi_2S_3 Nanostructures for Superior Visible-light-driven Cr(VI) Removal Capacity. *ChemistrySelect* **2018**, *3*, 7123–7128. [CrossRef]
40. Wang, Y.J.; Jin, J.R.; Chu, W.G.; Cahen, D.; He, T. Synergistic Effect of Charge Generation and Separation in Epitaxially Grown BiOCl/Bi_2S_3 Nano-Heterostructure. *ACS Appl. Mater. Interfaces* **2018**, *10*, 15304–15313. [CrossRef]
41. Subha, N.; Mahalakshmi, M.; Monika, S.; Neppolian, B. Novel CeO_2 and rGO decorated Bi_2S_3 nanorods for the enhanced solar hydrogen production. *Mater. Lett.* **2021**, *294*, 129782. [CrossRef]

42. Li, X.; Chen, J.T.; Li, H.L.; Li, J.T.; Xu, Y.T.; Liu, Y.J.; Zhou, J.R. Photoreduction of CO_2 to methanol over Bi2S3/CdS photocatalyst under visible light irradiation. *J. Nat. Gas Chem.* **2011**, *20*, 413–417. [CrossRef]
43. Gotsis, H.J.; Barnes, A.C.; Strange, P. Experimental and theoretical investigation of the crystal structure of CuS (covellite). *J. Phys. Condens. Matter* **1992**, *4*, 10461–10468. [CrossRef]
44. Xu, W.; Zhu, S.; Liang, Y.; Li, Z.; Cui, Z.; Yang, X.; Inoue, A. Nanoporous CuS with excellent photocatalytic property. *Sci. Rep.* **2015**, *5*, 18125. [CrossRef]
45. Hubert, Y.S.; Mathew, S.A.; Dhanavel, S.; Narayanan, V.; Stephen, A. Visible light driven photocatalytic activity of copper sulfide nanoparticles. *J. Indian Chem. Soc.* **2019**, *96*, 207–208.
46. Song, C.D.; Zhang, J.; Gao, Y.; Lu, Y.Y.; Wang, F.F. Synthesis Direct Z-Scheme CuS-WO3 Photocatalysts Based on an Element-Reaction Route and Their Photocatalytic Activity. *Acta Phys.-Chim. Sin.* **2017**, *33*, 1891–1897.
47. Kadi, M.W.; Mohamed, R.M.; Ismail, A.A.; Bahnemann, D.W. H2 production using CuS/g-C3N4 nanocomposites under visible light. *Appl. Nanosci.* **2020**, *10*, 223–232. [CrossRef]
48. Shifu, C.; Mingsong, J.; Yunguang, Y. Synthesis and Characterization of Ce2S3-ZnS-CuS Nanoparticles and Their Photocatalytic Activity. *J. Nanosci. Nanotechnol.* **2012**, *12*, 4898–4904. [CrossRef]
49. Lv, Z.; Cui, H.; Huang, H.; Li, X.; Wang, H.; Ji, G. Study of the electronic, bonding, elastic and acoustic properties of covellite via first principles. *J. Alloys Compd.* **2017**, *692*, 440–447. [CrossRef]
50. Frueh, A.J., Jr. The crystallography of silver sulfide, Ag_2S. *Z. Kristallogr. Kristallgeom. Kristallph. Kristallchem.* **1958**, *110*, 136–144. [CrossRef]
51. Evans, H.T., Jr. Crystal structure of low chalcocite. *Nature* **1971**, *232*, 69–70. [CrossRef]
52. Marshall, R.; Mitra, S.S. Optical properties of cuprous sulfide. *J. Appl. Phys.* **1965**, *36*, 3882–3883. [CrossRef]
53. Tang, Q.-Y.; Chen, W.-F.; Lv, Y.-R.; Yang, S.-Y.; Xu, Y.-H. Z-scheme hierarchical Cu_2S/Bi_2WO_6 composites for improved photocatalytic activity of glyphosate degradation under visible light irradiation. *Sep. Purif. Technol.* **2020**, *236*, 116243. [CrossRef]
54. Huang, H.; Li, F.; Wang, H.; Zheng, X. The size controlled synthesis of Cu_2S/P_{25} hetero junction solar-energy-materials and their applications in photocatalytic degradation of dyes. *RSC Adv.* **2017**, *7*, 50056–50063. [CrossRef]
55. Liu, Q.; Hong, X.; Zhang, X.; You, X.; Zhao, X.; Liu, X.; Ye, M. Hierarchical Cu2S nanorods with different crystal phases for asymmetrical supercapacitors and visible-light photocatalysis. *Dalton Trans.* **2018**, *47*, 15189–15196. [CrossRef]
56. Patil, S.B.; Kishore, B.; Manjunath, K.; Reddy, V.; Nagaraju, G. One step hydrothermal synthesis of novel Cu_2S-MoO_3 nanocomposite for lithium ion battery and photocatalytic applications. *Int. J. Hydrog. Energy* **2018**, *43*, 4003–4014. [CrossRef]
57. El-Nahass, M.M.; Farag, A.A.M.; Ibrahim, E.M.; Abd-El-Rahman, S. Structural, optical and electrical properties of thermally evaporated Ag_2S thin films. *Vacuum* **2004**, *72*, 453–460. [CrossRef]
58. Do, J.Y.; Chava, R.K.; Kim, Y.I.; Cho, D.W.; Kang, M. Fabrication of Ag based ternary nanocomposite system for visible-light photocatalytic hydrogen evolution reaction. *Appl. Surf. Sci.* **2019**, *494*, 886–894. [CrossRef]
59. Li, X.; Shen, D.; Liu, C.; Li, J.; Zhou, Y.; Song, X.; Huo, P.; Wang, H.; Yan, Y. Fabricated rGO-modified Ag_2S nanoparticles/g-C_3N_4 nanosheets photocatalyst for enhancing photocatalytic activity. *J. Colloid Interface Sci.* **2019**, *554*, 468–478. [CrossRef]
60. Lin, Y.; Han, D.; Li, Y.; Tan, L.; Liu, X.; Cui, Z.; Yang, X.; Li, Z.; Liang, Y.; Zhu, S.; et al. Ag_2S@WS_2 Heterostructure for Rapid Bacteria-Killing Using Near-Infrared Light. *ACS Sustain. Chem. Eng.* **2019**, *7*, 14982–14990. [CrossRef]
61. Sun, S.; Li, P.; Liang, S.; Yang, Z. Diversified copper sulfide (Cu_2-xS) micro-/nanostructures: A comprehensive review on synthesis, modifications and applications. *Nanoscale* **2017**, *9*, 11357–11404. [CrossRef] [PubMed]
62. Gerlach, W. Das Kalpha-Dublett nebst einer Neubestimmung der Gitterkonstanten einiger Krystalle. *Physik. Zeitschrift* **1922**, *23*, 114–120.
63. Martienssen, W.; Warlimont, H. (Eds.) *Springer Handbook of Condensed Matter and Materials Data*; Springer: Berlin/Heidelberg, Germany, 2005; ISBN 978-3-540-44376-6.
64. Lee, G.-J.; Wu, J. Recent developments in ZnS photocatalysts from synthesis to photocatalytic applications—A review. *Powder Technol.* **2017**, *318*, 8–22. [CrossRef]
65. Rao, H.B.; Lu, Z.W.; Liu, X.; Ge, H.W.; Zhang, Z.Y.; Zou, P.; He, H.; Wang, Y.Y. Visible light-driven photocatalytic degradation performance for methylene blue with different multi-morphological features of ZnS. *RSC Adv.* **2016**, *6*, 46299–46307. [CrossRef]
66. Huo, F.; Wang, Y.S.; You, C.; Deng, W.Q.; Yang, F.; Pu, Y. Phase- and size-controllable synthesis with efficient photocatalytic activity of ZnS nanoparticles. *J. Mater. Sci.* **2017**, *52*, 5626–5633. [CrossRef]
67. Tiwari, A.; Dhoble, S.J. Critical Analysis of Phase Evolution, Morphological Control, Growth Mechanism and Photophysical Applications of ZnS Nanostructures (Zero-Dimensional to Three-Dimensional): A Review. *Cryst. Growth Des.* **2017**, *17*, 381–407. [CrossRef]
68. Barote, M.A.; Yadav, A.A.; Masumdar, E.U. Synthesis, characterization and photoelectrochemical properties of n-CdS thin films. *Phys. B Condens. Matter* **2011**, *406*, 1865–1871. [CrossRef]
69. Yuan, Y.-J.; Chen, D.Q.; Yu, Z.-T.; Zou, Z.-G. Cadmium sulfide-based nanomaterials for photocatalytic hydrogen production. *J. Mater. Chem. A* **2018**, *6*, 11606–11630. [CrossRef]
70. Boonserm, A.; Kruehong, C.; Seithtanabutara, V.; Artnaseaw, A.; Kwakhong, P. Photoelectrochemical response and corrosion behavior of CdS/TiO_2 nanocomposite films in an aerated 0.5 M NaCl solution. *Appl. Surf. Sci.* **2017**, *419*, 933–941. [CrossRef]
71. Ning, X.F.; Lu, G.X. Photocorrosion inhibition of CdS-based catalysts for photocatalytic overall water splitting. *Nanoscale* **2020**, *12*, 1213–1223. [CrossRef]

72. Wu, Z.Y.; Zhao, G.H.; Zhang, Y.N.; Tian, H.Y.; Li, D.M. Enhanced Photocurrent Responses and Antiphotocorrosion Performance of CdS Hybrid Derived from Triple Heterojunction. *J. Phys. Chem. C* **2012**, *116*, 12829–12835. [CrossRef]
73. Torimoto, T.; Kontani, H.; Shibutani, Y.; Kuwabata, S.; Sakata, T.; Mori, H.; Yoneyama, H. Characterization of ultrasmall CdS nanoparticles prepared by the size-selective photoetching technique. *J. Phys. Chem. B* **2001**, *105*, 6838–6845. [CrossRef]
74. Abrahams, S.C.; Bernstein, J.L. Crystal Structure of Piezoelectric nonlinear-optic $AgGaS_2$. *J. Chem. Phys.* **1973**, *59*, 1625–1629. [CrossRef]
75. Caudillo-Flores, U.; Kubacka, A.; Berestok, T.; Zhang, T.; Llorca, J.; Arbiol, J.; Cabot, A.; Fernández-García, M. Hydrogen photogeneration using ternary $CuGaS_2$-TiO_2-Pt nanocomposites. *Int. J. Hydrog. Energy* **2020**, *45*, 1510–1520. [CrossRef]
76. Liu, Z.; Liu, J.; Huang, Y.; Li, J.; Yuan, Y.; Ye, H.; Zhu, D.; Wang, Z.; Tang, A. From one- dimensional to two-dimensional wurtzite $CuGaS_2$ nanocrystals: Non-injection synthesis and photocatalytic evolution. *Nanoscale* **2019**, *11*, 158–169. [CrossRef]
77. Kaga, H.; Tsutsui, Y.; Nagane, A.; Iwase, A.; Kudo, A. An effect of Ag(I)-substitution at Cu sites in $CuGaS_2$ on photocatalytic and photoelectrochemical properties for solar hydrogen evolution. *J. Mater. Chem. A* **2015**, *3*, 21815–21823. [CrossRef]
78. Ni, D.R.; Kuo, H.-Y.; Park, J.E.; Lee, T.S.; Sloman, S.-R.I.; Cava, R.J.; Bocarsly, A.B. Improved H2 Evolution in Quaternary SCIGS Chalcopyrite Semiconductors. *J. Phys. Chem. C* **2018**, *122*, 24512–24519. [CrossRef]
79. Yamato, K.; Iwase, A.; Kudo, A. Photocatalysis using a Wide Range of the Visible Light Spectrum: Hydrogen Evolution from Doped $AgGaS_2$. *ChemSusChem* **2015**, *8*, 2902–2906. [CrossRef] [PubMed]
80. Takayama, T.; Sato, K.; Fujimura, T.; Kojima, Y.; Iwase, A.; Kudo, A. Photocatalytic CO_2 reduction using water as an electron donor by a powdered Z-scheme system consisting of metal sulfide and an RGO-TiO_2 composite. *Faraday Discuss.* **2017**, *198*, 397–407. [CrossRef] [PubMed]
81. Dalui, A.; Thupakula, U.; Khan, A.H.; Ghosh, T.; Satpati, B.; Acharya, S. Mechanism of Versatile Catalytic Activities of Quaternary CuZnFeS Nanocrystals Designed by a Rapid Synthesis Route. *Small* **2015**, *11*, 1829–1839. [CrossRef]
82. Wang, R.; Yue, M.; Cong, R.; Gao, W.; Yang, T. Photocatalytic reduction of nitrate over chalcopyrite $CuFe_0.7Cr_0.3S_2$ with high N_2 selectivity. *J. Alloys Compd.* **2015**, *651*, 731–736. [CrossRef]
83. Ye, Y.; Zang, Z.; Zhou, T.; Dong, F.; Lu, S.; Tang, X.; Wei, W.; Zhang, Y. Theoretical and experimental investigation of highly photocatalytic performance of CuInZnS nanoporous structure for removing the NO gas. *J. Catal.* **2018**, *357*, 100–107. [CrossRef]
84. Kolny-Olesiak, J.; Weller, H. Synthesis and Application of Colloidal $CuInS_2$ Semiconductor Nanocrystals. *ACS Appl. Mater. Interfaces* **2013**, *5*, 12221–12237. [CrossRef] [PubMed]
85. Choubrac, L.; Lafond, A.; Guillot-Deudon, C.; Moelo, Y.; Jobic, S. Structure flexibility of the Cu_2ZnSnS_4 absorber in low-cost photovoltaic cells: From the stoichiometric to the copper-poor compounds. *Inorg. Chem.* **2012**, *51*, 3346–3348. [CrossRef] [PubMed]
86. Patel, S.B.; Gohel, J.V. Recent developments in Cu_2ZnSnS_4 (CZTS) preparation, optimization and its application in solar cell development and photocatalytic applications. In *Photocatalytic Nanomaterials for Environmental Applications*; Tayade, R.J., Ed.; Materials Research Foundations; Materials Research Forum LLC: Millersville, PA, USA, 2018; Volume 27, pp. 370–404, ISBN 9781945291593.
87. Monga, D.; Sharma, S.; Shetti, N.P.; Basu, S.; Reddy, K.R.; Aminabhavi, T.M. Advances in transition metal dichalcogenide-based two-dimensional nanomaterials. *Mater. Today Chem.* **2021**, *19*, 100399. [CrossRef]
88. Yuan, Y.; Guo, R.-T.; Hong, L.-F.; Ji, X.-Y.; Li, Z.-S.; Lin, Z.-D.; Pan, W.-G. Recent advances and perspectives of MoS_2-based materials for photocatalytic dyes degradation: A review. *Colloids Surf. A* **2021**, *611*, 125836. [CrossRef]
89. Liu, C.; Kong, C.; Zhang, F.-J.; Kai, C.-M.; Cai, W.-Q.; Sun, X.-Y.; Oh, W.-C. Research progress of defective MoS_2 for photocatalytic hydrogen evolution. *J. Korean Ceram. Soc.* **2021**, *58*, 135–147. [CrossRef]
90. Gardinier, C.F.; Chang, L.L.Y. Phase relationships in the systems Mo-Sn-S, W-Sn-S and Mo-W-S. *J. Less-Common Met.* **1978**, *61*, 221–229. [CrossRef]
91. Kalikhman, V.L. Characteristics of the crystal structure, electrophysical properties, and model of the valence band spectrum of laminar compounds of molybdenum disulfide type. *Acta Crystallogr. B* **1983**, *39*, 404–407.
92. Wildervanck, J.C.; Jellinek, F. Preparation and crystallinity of molybdenum and tungsten sulfides. *Z. Anorgan. Allgem. Chem.* **1964**, *328*, 309–318. [CrossRef]
93. Traill, R.J. A rhombohedral polytype of molybdenite. *Can. Mineral.* **1962**, *7*, 524–526.
94. Kam, K.K.; Parkinson, B.A. Detailed photocurrent spectroscopy of the semiconducting group-VI transition-metal dichalcogenides. *J. Phys. Chem.* **1982**, *86*, 463–467. [CrossRef]
95. Synnatschke, K.; Cieslik, P.A.; Harvey, A.; Castellanos-Gómez, A.; Tian, T.; Shih, C.-J.; Chernikov, A.; Santos, E.J.G.; Coleman, J.N.; Backes, C. Length- and Thickness-Dependent Optical Response of Liquid-Exfoliated Transition Metal Dichalcogenides. *Chem. Mater.* **2019**, *31*, 10049–10062. [CrossRef]
96. Wu, C.; Zhang, J.; Tong, X.; Yu, P.; Xu, J.-Y.; Wu, J.; Wang, Z.M.M.; Lou, J.; Chueh, Y.-L. A Critical Review on Enhancement of Photocatalytic Hydrogen Production by Molybdenum Disulfide: From Growth to Interfacial Activities. *Small* **2019**, *15*, 1900578. [CrossRef]
97. Wilcoxon, J.P.; Newcomer, P.P.; Samara, G.A. Synthesis and optical properties of MoS_2 and isomorphous nanoclusters in the quantum confinement regime. *J. Appl. Phys.* **1997**, *81*, 7934–7944. [CrossRef]
98. Thurston, T.R.; Wilcoxon, J.P. Photooxidation of organic chemicals catalyzed by nanoscale MoS_2. *J. Phys. Chem. B* **1999**, *103*, 11–17. [CrossRef]

99. Fang, Y.Q.; Pan, J.; He, J.Q.; Luo, R.C.; Wang, D.; Che, X.L.; Bu, K.J.; Zhao, W.; Liu, P.; Mu, G.; et al. Structure Re-determination and Superconductivity Observation of Bulk 1T MoS_2. *Angew. Chem. Int. Ed.* **2018**, *57*, 1232–1235. [CrossRef] [PubMed]
100. Shan, S.T.; Zhu, S.S.; Pan, Z.G.; Lu, Y.O.; Liu, Y.F.; Tao, Y.Q. Heteroepitaxial Growth of 1T MoS_2 Nanosheets on SnO_2 with Synergetic Improvement on Photocatalytic Activity. *Cryst. Res. Technol.* **2021**, *56*, 2000091. [CrossRef]
101. McTaggart, F.K.; Wadsley, A.D. The sulphides, selenides, and tellurides of titanium, zirconium, hafnium, and thorium. I. Preparation and characterization. *Austr. J. Chem.* **1958**, *11*, 445–457. [CrossRef]
102. Moustafa, M.; Zandt, T.; Janowitz, C.; Manzke, R. Growth and band gap determination of the $ZrSxSe_2$-x single crystal series. *Phys. Rev. B* **2009**, *80*, 035206. [CrossRef]
103. Li, S.; Wang, C.; Qiu, H. Single- and few-layer ZrS_2 as efficient photocatalysts for hydrogen production under visible light. *Int. J. Hydrog. Energy* **2015**, *40*, 15503–15509. [CrossRef]
104. Yue, X.F.; Liang, Y.; Jiang, J.; Liu, R.G.; Ren, S.T.; Gao, R.X.; Zhong, B.; Wen, G.W.; Wang, Y.Y.; Zou, M.Q. Raman intensity enhancement of molecules adsorbed onto HfS2 flakes up to 200 layers. *Nanoscale* **2019**, *11*, 2179–2185. [CrossRef]
105. Wang, B.; Wang, X.T.; Wang, P.; Yang, T.; Yuan, H.K.; Wang, G.Z.; Chen, H. Bilayer $MoSe_2/HfS_2$ Nanocomposite as a Potential Visible-Light-Driven Z-Scheme Photocatalyst. *Nanomaterials* **2019**, *9*, 1706. [CrossRef] [PubMed]
106. Paszkowicz, W.; Leiro, J.A. Rietveld refinement study of pyrite crystals. *J. Alloys Compd.* **2005**, *401*, 289–295. [CrossRef]
107. Qin, H.; Jia, J.; Lin, L.; Ni, H.; Wang, M.; Meng, L. Pyrite FeS_2 nanostructures: Synthesis, properties and applications. *Mater. Sci. Eng. B* **2018**, *236–237*, 104–124. [CrossRef]
108. Sakthi Sudar Saravanan, R.; Meena, M.; Pukazhselvan, D.; Mahadevan, C.K. Structural, optical and electrical characterization of Mn(2+) and Cd(2+) doped/co-doped PbS nanocrystals. *J. Alloys Compd.* **2015**, *627*, 69–77. [CrossRef]
109. Segets, D.; Lucas, J.M.; Klupp Taylor, R.N.; Scheele, M.; Zheng, M.; Alivisatos, A.P.; Peukert, W. Determination of the Quantum Dot Band Gap Dependence on Particle Size from Optical Absorbance and Transmission Electron Microscopy Measurements. *ACS Nano* **2012**, *6*, 9021–9032. [CrossRef] [PubMed]
110. Sun, J.; Li, Y.Z.; Yang, Y.; Bai, J.L.; Zhao, X.J. Effect of the interface on UV-vis-IR photodetection performance of PbS/ZnO nanocomposite photocatalysts. *Appl. Surf. Sci.* **2015**, *358*, 498–505. [CrossRef]
111. Zhang, X.L.; Tang, Y.H.; Li, Y.; Wang, Y.; Liu, X.N.; Liu, C.B.; Luo, S.L. Reduced graphene oxide and PbS nanoparticles co-modified TiO2 nanotube arrays as a recyclable and stable photocatalyst for efficient degradation of pentachlorophenol. *Appl. Catal. A* **2013**, *457*, 78–84. [CrossRef]
112. Steigmann, G.A.; Sutherland, H.H.; Goodyear, J. The crystal structure of β-In2S3. *Acta Crystallogr.* **1965**, *19*, 967–971. [CrossRef]
113. Shen, S.; Guo, L. Structural, textural and photocatalytic properties of quantum-sized In_2S_3-sensitized Ti-MCM-41 prepared by ion-exchange and sulfidation methods. *J. Solid State Chem.* **2006**, *79*, 2629–2635. [CrossRef]
114. Yang, X.; Xu, J.; Wong, T.L.; Yang, Q.D.; Lee, C.S. Synthesis of In_2O_3-In_2S_3 core-shell nanorods with inverted type-I structure for photocatalytic H_2 generation. *Phys. Chem. Chem. Phys.* **2013**, *15*, 12688–12693. [CrossRef] [PubMed]
115. Li, X.P.; Huang, R.J.; Chen, C.; Li, T.D.; Gao, Y.J. Simultaneous Conduction and Valence Band Regulation of Indium-Based Quantum Dots for Efficient H_2 Photogeneration. *Nanomaterials* **2021**, *11*, 1115. [CrossRef] [PubMed]
116. Du, W.; Zhu, J.; Li, S.; Qian, X. Ultrathin beta-In2S3 nanobelts: Shape-controlled synthesis and optical and photocatalytic properties. *Cryst. Growth Des.* **2008**, *8*, 2130–2136. [CrossRef]
117. He, Y.H.; Li, D.Z.; Xiao, G.C.; Chen, W.; Chen, Y.B.; Sun, M.; Huang, H.J.; Fu, X. A New Application of Nanocrystal In2S3 in Efficient Degradation of Organic Pollutants under Visible Light Irradiation. *J. Phys. Chem. C* **2009**, *113*, 5254–5262. [CrossRef]
118. Xie, M.L.; Dai, X.; Meng, S.G.; Fu, X.L.; Chen, S.F. Selective oxidation of aromatic alcohols to corresponding aromatic aldehydes using In_2S_3 microsphere catalyst under visible light irradiation. *Chem. Eng. J.* **2014**, *245*, 107–116. [CrossRef]
119. Gao, C.; Li, J.; Shan, Z.; Huang, F.; Shen, H. Preparation and visible-light photocatalytic activity of In_2S_3/TiO_2 composite. *Mater. Chem. Phys.* **2010**, *122*, 183–187. [CrossRef]
120. Li, Y.J.; Li, T.; Tian, J.; Wang, X.Z.; Cui, H.Z. TiO_2 Nanobelts Decorated with In_2S_3 Nanoparticles as Photocatalysts with Enhanced Full-Solar-Spectrum (UV-vis-NIR) Photocatalytic Activity toward the Degradation of Tetracycline. *Part. Part. Syst. Charact.* **2017**, *34*, 1700127. [CrossRef]
121. Chai, B.; Peng, T.; Zeng, P.; Mao, J. Synthesis of floriated In_2S_3 decorated with TiO_2 nanoparticles for efficient photocatalytic hydrogen production under visible light. *J. Mater. Chem.* **2011**, *21*, 14587–14593. [CrossRef]
122. Štengl, V.; Opluštil, F.; Němec, T. In^{3+}-doped TiO2 and TiO_2/In_2S_3 Nanocomposite for Photocatalytic and Stoichiometric Degradations. *Photochem. Photobiol.* **2012**, *88*, 265–276. [CrossRef]
123. Soni, V.; Raizada, P.; Kumar, A.; Hasija, V.; Singal, S.; Singh, P.; Hosseini-Bandegharaei, A.; Thakur, V.K.; Nguyen, V.H. Indium sulfide-based photocatalysts for hydrogen production and water cleaning: A review. *Environ. Chem. Lett.* **2021**, *19*, 1065–1095. [CrossRef]
124. Zhang, J.; Wang, H.; Yuan, X.; Zeng, G.; Tu, W.; Wang, S. Tailored indium sulfide-based materials for solar-energy conversion and utilization. *J. Photochem. Photobiol. C—Photochem. Rev.* **2019**, *38*, 1–26. [CrossRef]
125. Lucena, R.; Fresno, F.; Conesa, J.C. Spectral response and stability of In_2S_3 as visible light-active photocatalyst. *Catal. Commun.* **2012**, *20*, 1–5. [CrossRef]
126. Wang, W.; Zhu, W.; Zhang, L. A facile preparation and visible light-induced photocatalysis of indium sulfide superstructure. *Res. Chem. Intermed.* **2009**, *35*, 761–767. [CrossRef]

127. Lucena, R.; Conesa, J.C. Photocatalysis with octahedral sulfides. In *Current Developments in Photocatalysis and Photocatalytic Materials—New Horizons in Photocatalysis*; Wang, X., Anpo, M., Fu, X., Eds.; Elsevier: Amsterdam, The Netherlands, 2020; Chapter 24; pp. 385–403, ISBN 978-0-12-819000-5.
128. The Software VisualStat. Available online: http://www.visualstat.com/ (accessed on 12 April 2020).
129. Luque, A.; Martí, A. Increasing the efficiency of ideal solar cells by photon induced transitions at intermediate levels. *Phys. Rev. Lett.* **1997**, *78*, 5014–5017. [CrossRef]
130. Palacios, P.; Aguilera, I.; Sánchez, K.; Conesa, J.C.; Wahnón, P. Transition-metal-substituted indium thiospinels as novel intermediate-band materials: Prediction and understanding of their electronic properties. *Phys. Rev. Lett.* **2008**, *101*, 046403. [CrossRef]
131. Lucena, R.; Aguilera, I.; Palacios, P.; Wahnón, P.; Conesa, J.C. Synthesis and Spectral Properties of Nanocrystalline V-Substituted In2S3, a Novel Material for More Efficient Use of Solar Radiation. *Chem. Mater.* **2008**, *20*, 5125–5127. [CrossRef]
132. Lucena, R.; Conesa, J.C.; Aguilera, I.; Palacios, P.; Wahnón, P. V-substituted In2S3: An intermediate band material with photocatalytic activity in the whole visible light range. *J. Mater. Chem. A* **2014**, *2*, 8236–8245. [CrossRef]
133. Tapia, C.; Zacarias, S.; Pereira, I.A.C.; Conesa, J.C.; Pita, M.; De Lacey, A.L. In Situ Determination of Photobioproduction of H_2 by In_2S_3-[NiFeSe] Hydrogenase from Desulfovibrio vulgaris Hildenborough Using Only Visible Light. *ACS Catal.* **2016**, *6*, 5691–5698. [CrossRef]
134. Pita, M.; Mate, D.M.; González-Pérez, D.; Shleev, S.; Fernández, V.M.; Alcalde, M.; De Lacey, A.L. Bioelectrochemical Oxidation of Water. *J. Am. Chem. Soc.* **2014**, *136*, 5892–5895. [CrossRef]
135. Tapia, C.; Shleev, S.; Conesa, J.C.; De Lacey, A.L.; Pita, M. Laccase-Catalyzed Bioelectrochemical Oxidation of Water Assisted with Visible Light. *ACS Catal.* **2017**, *17*, 4881–4889. [CrossRef]
136. Donika, F.G.; Radautsan, S.I.; Kiosse, G.A.; Semiletov, S.A.; Donika, T.V.; Mustya, I.G. Crystal structure of the double-pack polytype $ZnIn_2S_4$(II), and more careful determination of the structure of the triple-pack polytype $ZnIn_2S_4$ (III). *Sov. Phys. Crystallogr.* **1971**, *16*, 190–192, reprinted in *Kristallografiya* **1971**, *16*, 235–237.
137. Donika, F.G.; Kiosse, G.A.; Radautsan, S.I.; Semiletov, S.A.; Mustya, I.G. Crystal structure of the two pack polytypic form $ZnIn_2S_4$(II). *Sov. Phys. Crystallogr.* **1972**, *17*, 575–577, reprinted in *Kristallografiya* **1972**, *17*, 663–665.
138. Biyushkina, A.V.; Donika, F.G.; Radautsan, S.I. Crystal structure of a six-stack polytype $ZnIn_2S_4$(VI). *Sov. Phys. Dokl.* **1989**, *34*, 402–404, reprinted in *Dokl. Akad. Nauk. SSSR* **1989**, *306*, 617–619.
139. Gou, X.; Cheng, F.; Shi, Y.; Zhang, L.; Peng, S.; Chen, J.; Shen, P. Shape-controlled synthesis of ternary chalcogenide $ZnIn_2S_4$ and $CuIn(S,Se)_2$ nano-/microstructures via facile solution route. *J. Am. Chem. Soc.* **2006**, *128*, 7222. [CrossRef] [PubMed]
140. Pan, Y.; Yuan, X.; Jiang, L.; Yu, H.; Zhang, J.; Wang, H.; Guan, R.; Zeng, G. Recent advances in synthesis, modification and photocatalytic applications of micro/nano-structured zinc indium sulfide. *Chem. Eng. J.* **2018**, *354*, 407. [CrossRef]
141. Lei, Z.; You, W.; Liu, M.; Zhou, G.; Takata, T.; Hara, M.; Domen, K.; Li, C. Photocatalytic water reduction under visible light on a novel $ZnIn_2S_4$ catalyst synthesized by hydrothermal method. *Chem. Commun.* **2003**, 2142–2143. [CrossRef] [PubMed]
142. Hu, X.; Yu, J.C.; Gong, J.; Li, Q. Rapid mass production of hierarchically porous $ZnIn_2S_4$ submicrospheres via a microwave-solvothermal process. *Cryst. Growth Des.* **2007**, *7*, 2444–2448. [CrossRef]
143. Chaudhari, N.S.; Bhirud, A.P.; Sonawane, R.S.; Nikam, L.K.; Warule, S.S.; Raneb, V.H.; Kale, B.B. Ecofriendly hydrogen production from abundant hydrogen sulfide using solar light-driven hierarchical nanostructured ZnIn2S4 photocatalyst. *Green Chem.* **2011**, *13*, 2500–2506. [CrossRef]
144. Song, Y.Y.; Zhang, J.Y.; Dong, X.H.; Li, H.D. A Review and Recent Developments in Full-Spectrum Photocatalysis using $ZnIn_2S_4$-Based Photocatalysts. *Energy Technol.* **2021**, *9*, 2100033. [CrossRef]
145. Hazen, R.M.; Finger, L.W. Crystal-Structures and Compressibilities of Layer Minerals at High-Pessure.1. SnS_2, Berndtite. *Am. Mineral.* **1978**, *63*, 289–292.
146. Günter, J.R.; Oswald, H.R. Neue polytype Form von Zinn(IV)-sulfid. *Naturwissenschaften* **1968**, *55*, 177. [CrossRef]
147. Eppelsheimer, D. Präparative und pulverroentgenographische Untersuchungen am System Sn-Sb-S. *Z. Krist.* **1981**, *156*, 36–37.
148. Greenaway, D.L.; Nitsche, R. Preparation and optical properties of group IV–VI2 chalcogenides having the CdI2 structure. *J. Phys. Chem. Solids* **1965**, *26*, 1445–1458. [CrossRef]
149. He, H.Y.; Huang, J.F.; Cao, L.Y.; Wu, J.R.; He, Z. Photocatalytic activity of mixture of SnS_2 and TiO_2 powders in destruction of metyhyl orange in water. *J. Optoelectron. Adv. Mater.* **2007**, *9*, 3781–3784.
150. Damkale, S.R.; Arbuj, S.S.; Umarji, G.G.; Panmand, R.P.; Khore, S.K.; Sonawane, R.S.; Rane, S.B.; Kale, B.B. Two-dimensional hexagonal SnS_2 nanostructures for photocatalytic hydrogen generation and dye degradation. *Sustain. Energy Fuels* **2019**, *3*, 3406–3414. [CrossRef]
151. Zhao, Y.; Sun, D.; Hu, K.; Zhao, W.; Huang, F. Surface defect engineering of SnS_2 nanocrystals for enhanced photocatalytic reduction of Cr(VI) under visible light. *Inorg. Chem. Commun.* **2020**, *114*, 107849. [CrossRef]
152. Makama, A.B.; Salmiaton, A.; Choong, T.S.Y.; Hamid, M.R.A.; Abdullah, N.; Saion, E. Influence of parameters and radical scavengers on the visible-light-induced degradation of ciprofloxacin in ZnO/SnS_2 nanocomposite suspension: Identification of transformation products. *Chemosphere* **2020**, *253*, 126689. [CrossRef]
153. She, H.; Zhou, H.; Li, L.; Zhao, Z.; Jiang, M.; Huang, J.; Wang, L.; Wang, Q. Construction of a Two-Dimensional Composite Derived from TiO_2 and SnS_2 for Enhanced Photocatalytic Reduction of CO_2 into CH_4. *ACS Sustain. Chem. Eng.* **2019**, *7*, 650–659. [CrossRef]

154. Han, A.; Li, M.; Zhang, S.; Zhu, X.; Han, J.; Ge, Q.; Wang, H. Ti^{3+} Defective SnS_2/TiO_2 Heterojunction Photocatalyst for Visible-Light Driven Reduction of CO_2 to CO with High Selectivity. *Catalysts* **2019**, *9*, 927. [CrossRef]
155. Lucena, R.; Fresno, F.; Conesa, J.C. Hydrothermally synthesized nanocrystalline tin disulphide as visible light-active photocatalyst: Spectral response and stability. *Appl. Catal. A Gen.* **2012**, *415–416*, 111–117. [CrossRef]
156. Wahnón, P.; Conesa, J.C.; Palacios, P.; Lucena, R.; Aguilera, I.; Seminovski, Y.; Fresno, F. V-doped SnS2: A new intermediate band material for a better use of the solar spectrum. *Phys. Chem. Chem. Phys.* **2011**, *13*, 20401–20407. [CrossRef] [PubMed]
157. Jarne, C.; Paul, L.; Conesa, J.C.; Shleev, S.; De Lacey, A.L.; Pita, M. Underpotential Photoelectrooxidation of Water by SnS_2-Laccase Co-catalysts on Nanostructured Electrodes with Only Visible-Light Irradiation. *ChemElectroChem* **2019**, *9*, 2755–2761. [CrossRef]
158. Zuo, Y.; Liu, Y.; Li, J.; Du, R.; Yu, X.; Xing, C.; Zhang, T.; Yao, L.; Arbiol, J.; Llorca, J.; et al. Solution-Processed Ultrathin SnS_2-Pt Nanoplates for Photoelectrochemical Water Oxidation. *ACS Appl. Mater. Interfaces* **2019**, *11*, 6918–6926. [CrossRef]
159. Xu, Y.; Schoonen, M.A.A. The absolute energy positions of conduction and valence bands of selected semiconducting minerals. *Am. Mineral.* **2000**, *85*, 543–556. [CrossRef]